A Robust Forced Dynamic Sliding Mode Minimum Energy Position Controller for Permanent Magnet Synchronous Motor Drives

STEPHEN J. DODDS, GUNARATNAM. SOORIYAKUMAR, ROY PERRYMAN
School of Computing and Technology,
University of East London,
University Way, London E16 2RD
UNITED KINGDOM
s.j.dodds@uel.ac.uk; soori@ctdynamics.com; r.perryman@uel.ac.uk

Abstract: As a contribution towards improving the environment, a new position controller for vector controlled electric drives employing permanent magnet synchronous motors (PMSM) is presented that achieves approximately 27% less frictional energy loss than a conventional controller adjusted to give the same manoeuvre time for the same initial and final positions. The frictional energy loss minimisation is carried out within the constraint of a velocity-time profile of fixed form to achieve prescribed manoeuvre times for relatively large step reference position changes. Optimal settings of the parameters of the velocity-time profile are made to minimise the energy loss. The control system robustness is achieved through the use of two control techniques, forced dynamic control (FDC) and sliding mode control (SMC), which maintain the velocity-time profile regardless of the mechanical load presented to the motor. The closed loop system automatically enters a linear operational mode with prescribed dynamics as the demanded position is approached, enabling derivative feed forward pre-compensation techniques to eliminate dynamic lag if needed. Vector control is achieved by an FDC direct axis current control loop with zero reference input, assuming a non-salient PMSM. The only information required from the user is the reference position and the required manoeuvre time. For commissioning, no time consuming adjustment of PI controllers is needed in contrast to conventional vector controlled drives. Only the following parametric entries are needed: a) the motor power and voltage ratings, the permanent magnet flux, the number of pole pairs and an estimate of the total moment of inertia presented to the rotor, to calculate the maximum rotor angular acceleration magnitude for which no motor control torque saturation can occur and b) the settling time for the FDC direct axis current control. Since a specified manoeuvre time may be realised, the method is especially suited to applications in which more than one position control loop has to be coordinated. The performance of the new controller and its advantages over a conventional controller adjusted to yield the same settling time are demonstrated by simulations.

Key-Words: Forced dynamic control, sliding mode control, synchronous motor drives, minimum energy manoeuvres.

1 Introduction

Vector controllers for PMSM drives used in motion control applications typically employ three PI controllers, one aimed at driving the direct axis stator current component to zero to keep the magnetic flux and stator current vectors mutually orthogonal for maximum torque efficiency (the vector control condition), one for an inner speed control loop (to guarantee sufficient damping for the position control) and another completing the outer position control loop. The velocity and position PI controllers have to be tuned to achieve an acceptable response to step position reference changes. This standard form of vector controller, however, suffers from some drawbacks, the most important in the context of this paper being unnecessarily high energy loss due to friction in the driven mechanism. This is due to the high initial velocity peaks in the step responses produced under the action of traditional linear controllers. No attempt is usually made to minimise this loss, especially in production line applications where throughput speed is of paramount importance. Maximising the manoeuvre time, however, minimises the energy expenditure for a given motion control system with given initial and final positions, because the power loss due to viscous friction increases with the square of the velocity. In this case the gains of the aforementioned standard PI controllers could be adjusted to yield the maximum tolerable manoeuvre time. In view of the aforementioned high velocity peaks, however, a lower minimum energy loss would be expected using a another form of controller designed especially for the purpose.

Ideally, an optimal controller should be found that yields the *absolute* minimum frictional energy loss for given initial and final positions. To arrive at a practicable controller, however, the manoeuvre time cannot be arbitrarily long and so one constraint is that

it is fixed at the maximum allowable value. Other constraints are imposed by the limitations of the hardware: The finite power supply voltages and the back e.m.f. of the machine combine to limit the stator currents and therefore limit the control torque magnitude. Also the peak speed of a manoeuvre has to be kept well below the value for which the back e.m.f. limits the stator currents to zero! Hence this optimal control problem is one of cost function minimisation for given initial and final plant states, subject to control saturation and state magnitude constraints and a fixed time to apply the control function. The general solution to this class of problem was produced by Pontryagin et al [9] but this is an open loop solution in which the optimal control function is computed 'of line' and subsequently applied to the plant in real time. This is impracticable for a number of reasons, the main one being that unknown external disturbances would cause the plant state trajectory to deviate from the planned optimal path *undetected*. In theory, this problem could be alleviated by equivalent closed loop optimal state feedback control laws, but their derivation in an algebraic form for implementation on a digital processor is intractable in all but a few simple cases such as the time optimal control of a double integrator plant [6]. Even if the closed form of a minimum energy state feedback control law were to be discovered, it would be based on a state space model of the plant and therefore could be sensitive to modelling errors. In principle, on line plant identification could alleviate this problem but the relatively high computational load would render this approach unattractive as a replacement for the existing PI controllers in industrial vector controlled electric drives. Minimum energy motion control has been attempted by Ma [1] who reports the aforementioned difficulties and approaches the problem with approximate model based optimal control. In contrast, the approach here is based on robust control techniques and to the knowledge of the authors is the first attempt at minimising energy loss in this way.

Although absolute minimisation of frictional energy loss is not attempted, the attainable performance of the proposed robust control law exceeds that of conventional vector controlled drives. The optimisation within the constraints of the chosen form of control law is relatively straightforward. Also the concept is fairly easily understood and its computational demands are well within the reach of modern digital processors of the type currently used in electric drives and therefore the new controller should be acceptable in industry.

2 Model of the PMSM and its Load

The state differential equations

$$di_d/dt = -Ai_d + B\omega_r i_q + Fu_d \quad (1)$$

$$di_q/dt = -\left(Ci_d + E\right)\omega_r - Di_q + Gu_q \quad (2)$$

$$d\theta_r/dt = \omega_r \quad (3)$$

$$d\omega_r/dt = \left(H + Ki_d\right)i_q - M\Gamma_L \quad (4)$$

model the PMSM in the synchronously rotating d-q co-ordinate system, together with its mechanical load, where i_d, i_q and u_d, u_q are the stator current and voltage components, ω_r and θ_r are the rotor angular velocity and angle, and Γ_L is the total load torque presented to the motor. The constant coefficients are:

$$\begin{cases} A = R_s/L_d; \quad B = pL_q/L_d; \quad C = pL_d/L_q; \\ D = R_s/L_q; \quad E = p\Psi_{PM}/L_q; \; F = 1/L_d; \quad G = 1/L_q; \\ H = 3p\Psi_{PM}/(2J_r); K = 3p\left(L_d - L_q\right)/(2J_r); M = 1/J_r \end{cases}$$

where Ψ_{PM} is the permanent magnet flux, R_S is the stator resistance, L_d and L_q are the direct and quadrature axis inductances, p is the number of pole pairs and J_r is the rotor moment of inertia.

The robustness introduced by the observer of subsection 3.4 may be understood by rewriting (4) as a torque balance equation two different ways. The first, which is used in the observer, is for the rotor inertial torque:

$$J_r \frac{d\omega_r}{dt} = \Gamma_{em} - \Gamma_L \quad (4a)$$

The second is for the total inertial torque:

$$\left(J_r + J_L\right)\frac{d\omega_r}{dt} = \Gamma_{em} - \left(F_v\omega_r + \Gamma_{Le}\right) \quad (4b)$$

where J_L is the load moment of inertia referred to the PMSM, $F_v\omega_r$ is the viscous friction assumed to be responsible for most of the energy loss, Γ_{Le} is the external load torque and Γ_{em} is the electromagnetic control torque:

$$\Gamma_{em} = (3p/2)\left[\Psi_{PM} + \left(L_d - L_q\right)i_d\right]i_q \quad (5)$$

Subtracting (4b) from (4a) then yields:

$$\Gamma_L = J_L\frac{d\omega_r}{dt} + F_v\omega_r + \Gamma_{Le} \quad (6)$$

As will be seen, Γ_L is counteracted by the controller using an accurate estimate of this from the

observer. So there is no need to model any of the terms on the RHS of (6). This gives the FDC its robustness.

3 Inner Forced Dynamic Control Loops

3.1 Overview

Forced dynamic control (FDC) is a general control method extending to nonlinear multivariable plants [3]. It forces the closed loop system to follow prescribed dynamics and is closely related to feedback linearisation [9] but differs in that it directly takes external disturbances into account. As already mentioned, this feature gives FDC robustness through use of an observer for estimation of the total load torque. As will be seen, the load torque derivative is also needed and a good example of this is given in [11]. The control system to be formulated employs FDC for control of the direct axis current, i_d, and the rotor angular acceleration

$$\alpha = \left(H + Ki_d\right)i_q - M\Gamma_L \tag{7}$$

with u_d and u_q as the control variables. To keep the current and magnetic flux vectors mutually perpendicular for maximum torque efficiency (i.e., the vector control condition) the direct axis stator current component is controlled with the demanded value set to $i_{d\_dem} = 0$. The FDC angular acceleration control loop is treated as an inner loop for the rotor angle control with the demanded angular acceleration, a_{dem}, as the control variable, as presented in subsection 3.6.

3.2 Direct axis stator current control

By inspection of (1), the control variable, u_d, appears on the RHS and therefore the rank of the plant with respect to i_d is just 1 and so the desired closed loop differential equation is of first order. Choosing this as linear with a settling time of T_{si} to 95% of the steady state step response (i.e., the classical 5% criterion) yields:

$$\frac{di_d}{dt} = \frac{3}{T_{si}}\left(i_{d\_dem} - i_d\right) \tag{8}$$

$i_d(t)$ is then *forced* to have the dynamics of (8) by equating the RHS of (1) to the RHS of (8) and then solving the resulting equation for u_d. Thus the forced dynamic direct axis current control law is:

$$u_d = \frac{1}{F}\left[\frac{3}{T_{si}}\left(i_{d\_dem} - i_d\right) + Ai_d - B\omega_r i_q\right] \tag{9}$$

The vector control condition requires

$$i_{d\_dem} = 0 \tag{10}$$

3.3 Rotor angular acceleration control

It is clear from (7) that there is no direct algebraic dependence of α on u_d or u_q. Hence (7) is differentiated:

$$\frac{d\alpha}{dt} = \left(H + Ki_d\right)\frac{di_q}{dt} + Ki_q\frac{di_d}{dt} - M\frac{d\Gamma_L}{dt} \tag{11}$$

Substituting for di_d/dt and di_q/dt in (11) using, respectively, (1) and (2) then yields:

$$\begin{cases} \dfrac{d\alpha}{dt} = \left(H + Ki_d\right)\left(-C\omega_r i_d - Di_q - E\omega_r + Gu_q\right) \\ \qquad\qquad + Ki_q\left(-Ai_d + B\omega_r i_q + Fu_d\right) - M\dfrac{d\Gamma_L}{dt} \end{cases} \tag{12}$$

Since both u_d and u_q now appear on the RHS of (12), the rank of the plant with respect to α is the order of the derivative on the LHS of (12), which is 1. The desired closed loop differential equation is therefore of first order and if this is chosen to be linear with a settling time of T_{sa} (5% criterion), then

$$\frac{d\alpha}{dt} = \frac{3}{T_{sa}}\left(\alpha_{d\_dem} - \alpha\right). \tag{13}$$

The control law is found by equating the RHS of (12) to the RHS of (13) and solving the resulting equation for u_q, noting that u_d is now known from (9):

$$\begin{aligned} &\left(H + Ki_d\right)\left(-C\omega_r i_d - Di_q - E\omega_r + Gu_q\right) \\ &\qquad + Ki_q\left(-Ai_d + B\omega_r i_q + Fu_d\right) \\ &\qquad - M\frac{d\Gamma_L}{dt} = \frac{3}{T_{sa}}\left(\alpha_{dem} - \alpha\right) \Rightarrow \end{aligned}$$

$$u_q = \frac{1}{G}\left\{\frac{\left[\begin{array}{l}\dfrac{3}{T_{s\alpha}}\left(\alpha_{dem} - \alpha\right) \\ + Ki_q\left(Ai_d - B\omega_r i_q - Fu_d\right) + M\dfrac{d\Gamma_L}{dt}\end{array}\right]}{H + Ki_d} + \left(C\omega_r i_d + Di_q + E\omega_r\right)\right\} \tag{14}$$

It should be noted that α may be calculated using (7) together with the known motor parameters and current measurements, an estimate of the load torque, Γ_L, being obtained from the observer presented in subsection 3.4.

If T_{sa} is chosen very much less than the minimum manoeuvre time, then the dynamic lag of the control loop is negligible and $\alpha \cong \alpha_{dem}$. The plant equation for the outer position loop can then be taken as

$$\ddot{\theta}_r = u \tag{15}$$

where $u = \alpha_{dem}$ is the control variable.

3.4 Observer

The main purpose of the observer is to estimate Γ_L and $d\Gamma_L/dt$ as needed by control law (14) and (7) but it also produces estimates of θ_r and $d\theta_r/dt$ which can be useful in applications where the measurement of θ_r is contaminated by significant measurement noise, in view of its filtering properties.

Γ_L and $d\Gamma_L/dt$ are treated as state variables in the real time plant model of the observer and in the absence of knowledge of the time variation of Γ_L , it is assumed that $d\Gamma_L^2/dt^2 = 0$. This does not impose a serious limitation provided the observer eigenvalues are sufficiently large to reduce the dynamic lag between $\Gamma_L(t)$ and $d\Gamma_L(t)/dt$ and their estimates to negligible proportions. The real time model consists of (3) and (4) together with the two load torque state equations, $dL_0/dt = L_1$ and $dL_1/dt = 0$, where $L_0 = \Gamma_L$ and $L_1 = d\Gamma_L/dt$. The corresponding observer equations are as follows, where the hats denote estimates of the variables above which they are placed:

$$\begin{cases} e_o = \hat{\theta}_r - \theta_r \\ d\hat{\theta}_r/dt = \omega_r + K_1 e_o \\ d\hat{\omega}_r/dt = (H + Ki_d)i_q - M\hat{L}_0 + K_2 e_o \\ d\hat{L}_0/dt = \hat{L}_1 + K_3 e_o \\ d\hat{L}_1/dt = K_4 e_o \end{cases} \tag{15}$$

The corresponding block diagram is shown in Fig. 1. The observer can be designed by eigenvalue placement in which case the characteristic equation is given by $\Delta(s) = 0$ where $\Delta(s)$ is the determinant of Mason's formula:

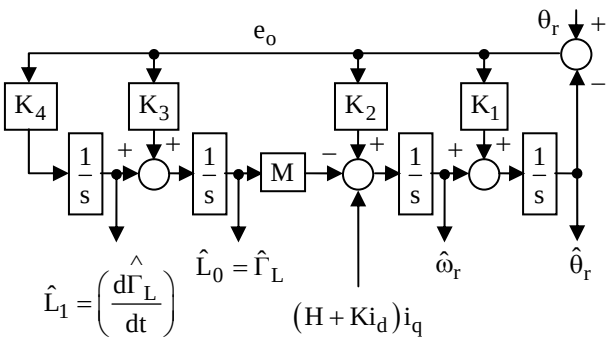

Fig. 1: Observer for estimation of Γ_L and $d\Gamma_L/dt$.

$$1 - \left[-\frac{K_1}{s} - \frac{K_2}{s^2} + \frac{K_3 M}{s^3} + \frac{K_4 M}{s^4} \right] = 0 \Rightarrow$$

$$s^4 + K_1 s^3 + K_2 s^2 - K_3 M s - K_4 M = 0 \tag{16}$$

Applying the Dodds 5% settling time formula [4] to the observer, i.e., $T_{so} = 1.5(1+n)T_{co}$, where n is the system order, for all the correction loop eigenvalues placed at $s = -1/T_{co}$, yields the desired characteristic equation:

$$\left[s + \frac{1.5(1+n)}{T_{s0}} \right]^n \Bigg|_{n=4} = \left(s + \frac{15}{2T_{s0}} \right)^4 = 0 \Rightarrow$$

$$s^4 + 4qs^3 + 6q^2 s^2 + 4q^3 s + q^4 = 0 \tag{17}$$

where $q = \dfrac{15}{2T_{so}}$. Comparing the LHS of (15) with that of (17) then yields the required observer correction loop gains:

$$\left\{ K_1 = 4q,\ K_2 = 6q^2,\ K_3 = -\frac{4q^3}{M},\ K_4 = -\frac{q^4}{M} \right\} \tag{18}$$

The smaller T_{s0} is made, then the more accurate $\hat{\Gamma}_L(t)$ and $\dot{\hat{\Gamma}}_L(t)$ will be. As stated at the end of section 2, the mechanical load is excluded from the real time model of the observer but its presence is reflected as a time varying load torque component which is compensated by the FDC algorithm through the terms containing $\hat{\Gamma}_L(t)$ [ref., (7)] and $\dot{\hat{\Gamma}}_L(t)$ [ref., (14)]. This yields robustness against external disturbances and plant model uncertainties that is fully exploited in the general control technique of observer based robust control [7] and applied in motion control [8].

4 Minimum Energy Position Control

4.1 Outer sliding mode position control loop

4.1.1 The plant and its state trajectory equation

The controlled plant for the outer loop is given by (15) and for a rest to rest manoeuvre, the demanded rotor angle, $\theta_{r\,dem}$, is constant. Then the position error, $\theta_{re} = \theta_r - \theta_{r\,dem}$, satisfies $\dot{\theta}_{re} = \dot{\theta}_r$ and $\ddot{\theta}_{re} = \ddot{\theta}_r$. The plant equation (15) can then be written as

$$\ddot{\theta}_r = u \tag{19}$$

and the plant state differential equations in terms of the state variables, θ_{re} and ω_r, are:

$$\begin{cases} \dot{\theta}_{re} = \omega_r \\ \dot{\omega}_r = u \end{cases} \tag{20}$$

In the basic form of sliding mode control, the control variable, u, is switched between one of two constant values, in this case, the maximum allowable angular acceleration limits, $\pm\alpha_{max}$. In the following subsection, the plant behaviour under this control law will be viewed by means of the state trajectories in the phase plane. These are solutions to the state trajectory differential equation which is obtained by dividing the first of equations (20) by the second:

$$\frac{d\theta_r}{d\omega_r} = \frac{\omega_r}{u} \tag{21}$$

The general state trajectory equation for u constant is obtained by the method of separation of variables:

$$\int u\, d\theta_{re} = \int \omega_r d\omega_r \Rightarrow$$

$$\theta_{re} = \theta_{re}(0) + \frac{1}{2u}\left[\omega_r^2 - \omega_r^2(0)\right]. \tag{22}$$

Thus the state trajectories are parabolas symmetrical about the θ_{re} axis of the phase plane with constant acceleration parameters, $u = \pm\alpha_{max}$, as shown in Figure 2 of the following subsection.

4.1.1 Basic bang-sliding mode control law

Sliding mode control [5] usually employs a linear switching boundary in the state space in order to obtain linear closed loop dynamics [5]. Here, in contrast, realisation of the special velocity-time control profile [ref., section 4.2] can be achieved by means of a special sliding mode control law having a piecewise linear switching boundary in the phase plain comprising a linear segment at the origin with slope $-1/T_c$, similar to the conventional sliding mode controller [5], and completed with two horizontal straight line segments as shown in Fig. 2. Here, ω_p is the peak angular velocity, which is the constant value reached during the manoeuvre, calculated to realise the demanded manoeuvre time, as shown in subsection 4.2. As will be seen later in this subsection, ideally the control acceleration magnitude limit, α_{max}, should be given the maximum possible value that can be held constant.

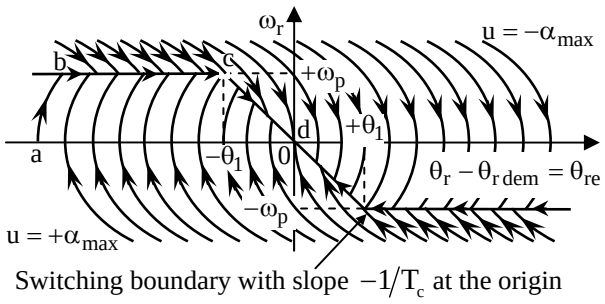

Fig. 2: Switching boundary for minimum energy loss control law and the closed loop phase portrait.

Below the switching boundary, $u = +\alpha_{max}$, and above, $u = -\alpha_{max}$, as shown, yielding the closed loop phase portrait comprising two families of parabolas with oppositely signed acceleration parameters. The phase portrait is actually an infinite continuum of state trajectories represented by a few sample trajectories in Fig. 2. The trajectories are directed towards the boundary from both sides, which is Utkin's condition for sliding motion [5]. Once the state trajectory reaches and just crosses the boundary, the control law holds it on the boundary by switching the control variable, u, at an infinite frequency in theory, between, causing it to 'zig-zag' about the boundary with an infinitesimal amplitude. Since the position error and the velocity are oppositely signed along the whole boundary then the state trajectory appears to *slide* along the boundary towards the origin and the system is said to be operating in a *sliding mode*. It is evident that for any initial state, the state trajectory is driven onto the boundary with $u = \pm\alpha_{max}$ and thereafter slides to the origin.

The closed-loop state trajectory a-b-c-d exemplifies a rest-to-rest manoeuvre. The control saturates at $u = +\alpha_{max}$ along segment a-b, after which $\omega_r = \omega_p$ is maintained along segment b-c and finally maintains $\omega_r = -(1/Tc)\theta_{re} \Rightarrow \dot{\theta}_r = (1/Tc)(\theta_{r\,dem} - \theta_r)$ along segment c-d, which therefore yields a linear closed loop system with transfer function

$$\frac{\theta_r(s)}{\theta_{r\,dem}(s)} = \frac{1}{1 + sTc} \tag{23}$$

With reference to Fig. 2, next the equation of the switching boundary will be found in the form

$$S(\theta_{re}, \omega_r) = 0 \tag{39}$$

Then the switching function is $S(\theta_{re}, \omega_r)$ and is arranged such that if ω_r is increased beyond the value on boundary (39) without changing θ_{re}, then $S(\theta_{re}, \omega_r) > 0$, and vice versa so that the required control law becomes:

$$u = -\alpha_{max}\, \mathrm{sgn}\left[S(\theta_{re}, \omega_r)\right] \tag{40}$$

Proceeding in this way for the example of Fig. 2, the switching boundary is defined by

$$\omega_r = \begin{cases} -\omega_p\, \mathrm{sgn}(\theta_{re}) \text{ for } |\theta_{re}| \geq T_c\omega_p \\ -\theta_{re}/T_c \text{ for } |\theta_{re}| < T_c\omega_p \end{cases} \tag{41}$$

where $\mathrm{sgn}(x) \overset{\Delta}{=} \begin{cases} +1 \text{ for } x > 0 \\ -1 \text{ for } x < 0 \end{cases}$, 0 for $x = 0$.

Equation (41) may be rewritten as

$$\omega_r = -\frac{1}{2}\left\{\begin{array}{l} \left[1 + \mathrm{sig}\left(|\theta_{re}| - T_c\omega_p\right)\right]\omega_p\, \mathrm{sgn}(\theta_{re}) \\ +\left[1 - \mathrm{sig}\left(|\theta_{re}| - T_c\omega_p\right)\right](\theta_{re}/T_c) \end{array}\right\} \tag{43}$$

where $\mathrm{sig}(x) \overset{\Delta}{=} \{+1 \text{ for } x \geq 0, -1 \text{ for } x < 0\}$.

Then the switching function of control law (40) follows from (43):

$$S(\theta_{re}, \omega_r) = \omega_r + \frac{1}{2}\left\{\begin{array}{l} \left[1 + \mathrm{sig}\left(|\theta_{re}| - T_c\omega_p\right)\right]\omega_p\, \mathrm{sgn}(\theta_{re}) \\ +\left[1 - \mathrm{sig}\left(|\theta_{re}| - T_c\omega_p\right)\right](\theta_{re}/T_c) \end{array}\right\} \tag{44}$$

4.1.2 Introduction of a boundary layer

As it stands, the outer loop control law derived in section 4.1.1 would suffer from *control chatter* [2]. This may be avoided by replacement of the switching boundary with the well-known *boundary layer* [1,4], i.e., a region straddling the switching boundary within which the control undergoes a continuous transition between $+\alpha_{max}$ and $-\alpha_{max}$ at the edges. This could be termed 'soft switching'. The boundary layer is introduced by replacing the signum function, $\mathrm{sgn}(\bullet)$, of (40) by the saturation function:

$$\mathrm{sat}(S, K) \triangleq \begin{cases} KS \text{ for } |S| < 1/K \\ \mathrm{sgn}(S) \text{ for } |S| \geq 1/K \end{cases} \tag{45}$$

Thus, (40) is replaced by

$$u = -\alpha_{max}\, \mathrm{sat}\left[S(\theta_{re}, \omega_r), K\right] \tag{46}$$

Fig. 3 shows a sketch of the basic and modified switching boundaries together with the boundary layer and a state trajectory for a rest-to-rest manoeuvre.

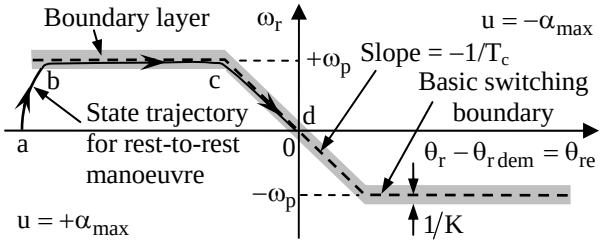

Fig. 3: Boundary layer and state trajectory.

The initial segment, a-b, of the state trajectory is the same as that of Fig. 2 with $u = +\alpha_{max}$ until the boundary layer is reached. Thereafter control law (46) keeps the trajectory within the boundary layer with a smooth control variable closely approaching the 'instantaneous mean value' of the bang-bang control of Fig. 2, i.e., the equivalent control of Utkin [5]. It is evident that as the gain, K, is increased, the width, $1/K$, of the boundary layer measured parallel to the ω_r axis becomes smaller and the state trajectory approaches closer to the ideal one of Fig. 2. In practice, however, the maximum value of K will be limited by the sampling frequency of the digital implementation but modern digital processors should allow this to be sufficiently high for the state trajectory to be a very close to the ideal one.

4.2 The velocity-time profile and the optimisation

Fig. 4 shows the angular velocity-time profile for a rest-to-rest manoeuvre produced by the forced dynamic sliding mode controller defined in subsections 3.3 and 4.1.

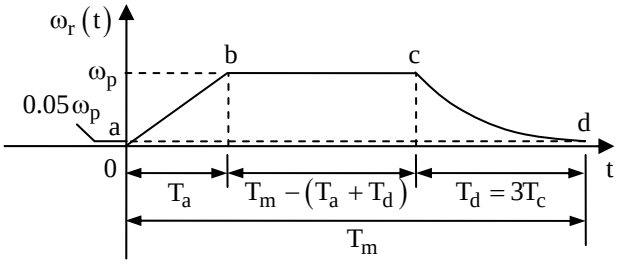

Fig. 4: Velocity-time profile for rest-to-rest manoeuvre.

The points, a, b, c and d, correspond to points, a, b, c and d, on the state trajectories of Fig. 2 and Fig. 3.

The torque required to overcome viscous friction is $\Gamma_f(t) = F_v \omega_r(t)$, where F_v is the viscous friction coefficient. Then, referring to Fig. 4, the energy loss during a manoeuvre of duration, T_m, is:

$$\begin{aligned} W_L &= \int_0^{T_m} F_v \omega_r^2(t)\,dt \\ &= F_v \left\{ \int_0^{T_a} \left(\frac{\omega_p}{T_a} \tau_a \right)^2 d\tau_a + \int_0^{T_m-(T_a+T_d)} \omega_p^2 d\tau_o \right. \\ &\qquad \left. + \int_0^{T_d} \left[\omega_p e^{-3\tau_d/T_d} \right]^2 d\tau_d \right\} \\ &= F_v \omega_p^2 \left[T_m - \tfrac{2}{3} T_a - \tfrac{1}{6}\left(5+e^{-6}\right) T_d \right] \end{aligned} \quad (47)$$

At the end of this manoeuvre, the position change has to be the demanded value of

$$\Delta\theta_{r\,dem} = \theta_{r\,dem} - \theta_r(0) \quad (48)$$

By inspection of Fig. 4 this is

$$\begin{aligned} \Delta\theta_{r\,dem} &= \int_0^{T_m} \omega_r(t)\,dt \\ &= \int_0^{T_a} \frac{\omega_p'}{T_a} \tau_a d\tau_a + \int_0^{T_m-(T_a+T_d)} \omega_p' d\tau_o \\ &\qquad + \int_0^{T_d} \omega_p' e^{-3\tau_d/T_d} d\tau_d \\ &= \omega_p' \left\{ T_m - \tfrac{1}{2} T_a - \tfrac{1}{3}\left(2+e^{-3}\right) T_d \right\} \end{aligned} \quad (49)$$

where $\omega_p' = \omega_p \,\mathrm{sgn}(\Delta\theta_r)$. Hence the required peak angular velocity magnitude is

$$\omega_p = \frac{\left|\Delta\theta_{r\,dem}\right|}{T_m - \tfrac{1}{2} T_a - \tfrac{1}{3}\left(2+e^{-3}\right) T_d} \quad (50)$$

Substituting for ω_p in (47) using (50) then yields

$$W_L = A \frac{T_m - \tfrac{2}{3} T_a - \tfrac{1}{6}\left(5+e^{-6}\right) T_d}{\left[T_m - \tfrac{1}{2} T_a - \tfrac{1}{3}\left(2+e^{-3}\right) T_d \right]^2} \quad (51)$$

where $A = F_v \left(\Delta\theta_{r\,dem}\right)^2$. Next, it is reasonable to suppose that the acceleration and deceleration levels will be of similar magnitude. This is satisfied by setting the peak initial deceleration equal and opposite to the constant acceleration and this is achieved by setting $T_d = 3T_a$. Then (51) becomes

$$W_L(T_a) = A \frac{T_m - \tfrac{1}{6}\left(19+3e^{-6}\right) T_a}{\left[T_m - \tfrac{1}{2}\left(5+2e^{-3}\right) T_a \right]^2} \quad (52)$$

and the intermediate period of constant velocity, ω_p, is $T_m - 4T_a$. Now the value of T_a that minimises W_L of (52) will be found. For this purpose, the minimum value will be taken as zero, although not realisable. The maximum value is $T_{a\,max} = \tfrac{1}{4} T_m$. Then

$$W_L(0) = A/T_m \quad (53)$$

$$W_L\left(\tfrac{1}{4} T_m\right) = \frac{A}{T_m} \frac{1 - \tfrac{1}{24}\left(19+3e^{-6}\right)}{\left[1 - \tfrac{1}{8}\left(5+2e^{-3}\right)\right]^2} = \frac{1.5826A}{T_m} \quad (54)$$

To find any stationary points, (52) will be rewritten:

$$\begin{aligned} &\left[T_m - \tfrac{1}{2}\left(5+2e^{-3}\right) T_a \right]^2 W_L(T_a) \\ &\qquad = A \left[T_m - \tfrac{1}{6}\left(19+3e^{-6}\right) T_a \right] \end{aligned} \quad (55)$$

Differentiating w.r.t. T_a then yields

$$\begin{aligned} &2\left[T_m - \tfrac{1}{2}\left(5+2e^{-3}\right) T_a \right] \left[-\tfrac{1}{2}\left(5+2e^{-3}\right) \right] W_L(T_a) \\ &\qquad + \left[T_m - \tfrac{1}{2}\left(5+2e^{-3}\right) T_a \right]^2 \frac{dW_L(T_a)}{dT_a} \\ &\qquad = -\tfrac{1}{6}\left(19+3e^{-6}\right) A \end{aligned} \quad (56)$$

Then setting $dW_L(T_a)/dT_a = 0$ and substituting for $W_L(T_a)$ using (52) yields

$$\begin{aligned} &\left[-\left(5+2e^{-3}\right) \right] \left[T_m - \tfrac{1}{6}\left(19+3e^{-6}\right) T_a \right] \\ &\qquad = -\tfrac{1}{6}\left(19+3e^{-6}\right) \left[T_m - \tfrac{1}{2}\left(5+2e^{-3}\right) T_a \right] \end{aligned}$$

Since this equation is linear in T_a, there is only one stationary point. Setting $T_a = 0$ in (56) and observing (53) yields:

$$T_m^2\, dW_L(T_a)/dT_a\big|_{T_a=0} = \tfrac{1}{6}\left(11 - 3e^{-6} + 12e^{-3}\right) A \quad (56)$$

Since $dW_L(T_a)/dT_a\big|_{T_a=0}$, $W_L\left(\tfrac{1}{4} T_m\right) > W_L(0)$ [ref., (52) and (53)] and there is at most one stationary point in the interval $0 \le T_a \le \tfrac{1}{4} T_m$, then the absolute minimum of $W_L(T_a)$ must be at

$T_a = 0$. It follows that the smallest value of T_a must be employed for which the electromagnetic control torque from the PMSM will not saturate. Then the FDC inner loop will be able to hold the initial angular acceleration at $\pm\alpha_{max} = \omega_p / T_{a\,min}$.

4.3 User inputs and parameter calculations

The user will provide a demanded manoeuvre time, T_m and a demanded rotor angle, $\theta_{r\,dem}$. Then the demanded rotor angle change, $\Delta\theta_{r\,dem}$, is given by (48). Then with $T_d = 3T_a$, (50) becomes

$$\omega_p = \frac{\left|\Delta\theta_{r\,dem}\right|}{T_m - \frac{1}{2}\left(5 + 2e^{-3}\right)T_a} \tag{57}$$

At commissioning time, the maximum angular acceleration magnitude, α_{max}, will be determined. Then

$$T_a = \omega_p / \alpha_{max} \tag{58}$$

Also the sliding mode time constant for the deceleration phase of a rest-to-rest manoeuvre and any subsequent operation with continuously varying position demands is set to

$$T_c = T_a \tag{59}$$

Substituting for T_a in (57) using (58) yields:

$$\tfrac{1}{2}\left(5 + 2e^{-3}\right)\omega_p^2 - \alpha_{max} T_m \omega_p + \alpha_{max}\left|\Delta\theta_{r\,dem}\right| = 0 \Rightarrow$$

$$\omega_p = \frac{\alpha_{max} T_m - \sqrt{\alpha_{max}^2 T_m^2 - 2\left(5 + 2e^{-3}\right)\alpha_{max}\left|\Delta\theta_{r\,dem}\right|}}{\left(5 + 2e^{-3}\right)} \tag{60}$$

the chosen root being the one yielding $\omega_p = 0$ for $\Delta\theta_{r\,dem} = 0$.

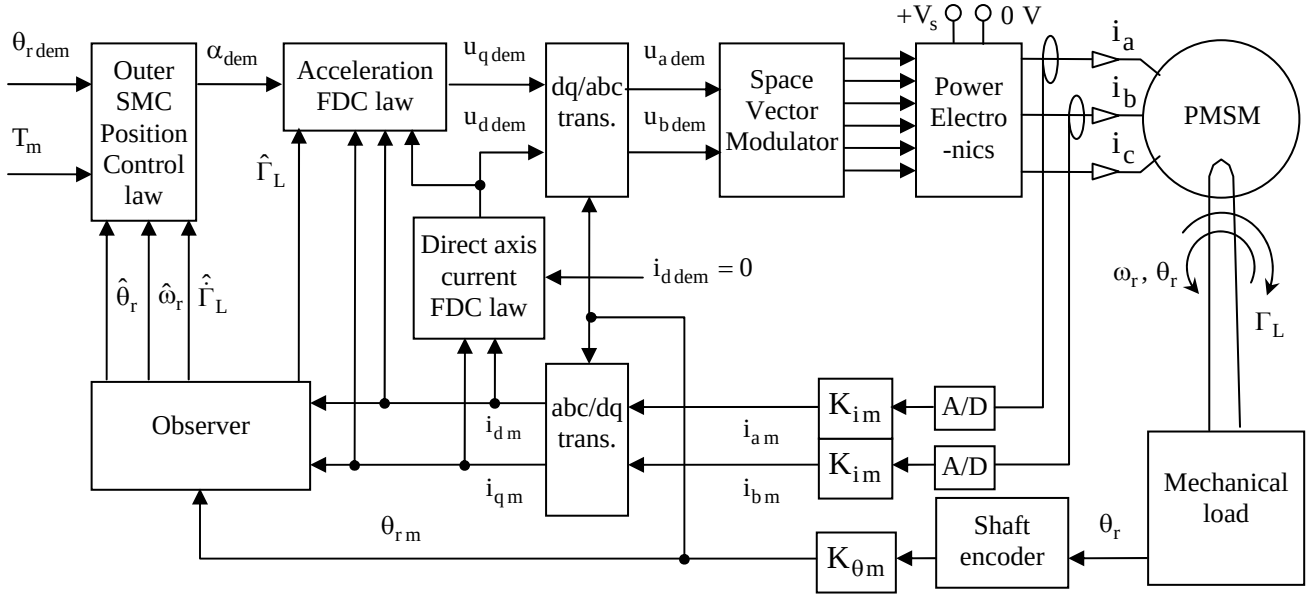

Fig. 5: Position control system under investigation.

5 Simulations

Fig. 5 shows the structure of the complete position control system as envisaged for future implementation.

Since for most applications the energy transmitted to the mechanical load will far exceed the losses in the PMSM and its drive, for this investigation the power electronics is assumed ideal, the space vector modulation not being simulated, and the iron losses in the PMSM are ignored. Also the measurement instrumentation is assumed ideal.

In this case, the applied stator voltages are equal to the demanded values, i.e., $u_a = u_{a\,dem}$, $u_b = u_{b\,dem}$, $u_c = -\left(u_{a\,dem} + u_{b\,dem}\right)$ and the measured currents and rotor angle are equal to the true values, i.e., $i_{a\,m} = i_a$, $i_{b\,m} = i_b$ and $\theta_{r\,m} = \theta$.

The total energy consumed is calculated as

$$W = 1.5\left(u_q i_q + u_d i_d\right) \tag{58}$$

and therefore this includes the PMSM copper losses.

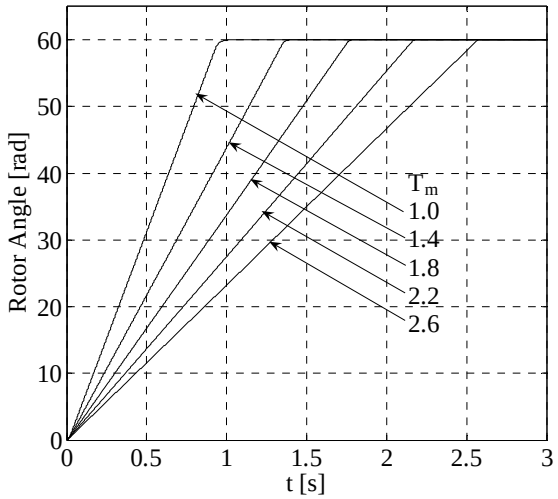

Fig. 6: Position responses with robust FDSMC for different manoeuvre times.

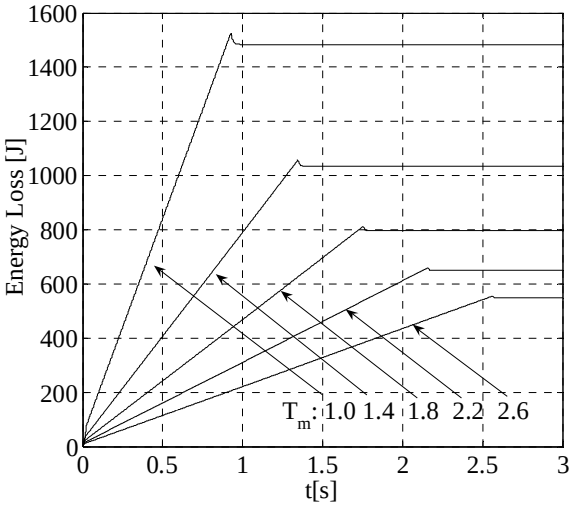

Fig. 7: Energy loss with robust FDSMC for different manoeuvre times.

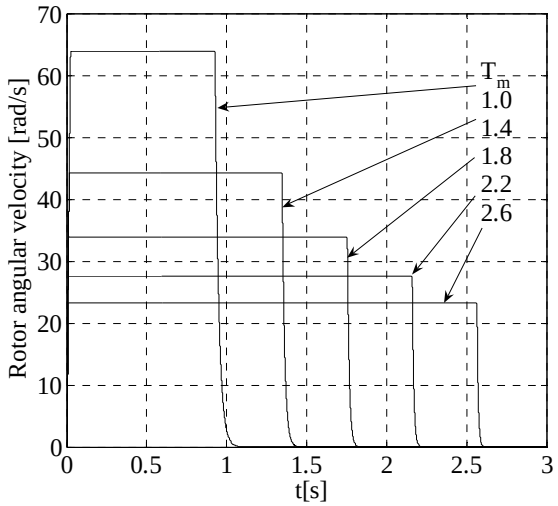

Fig. 8: Velocity-time profiles with robust FDSMC for different manoeuvre times.

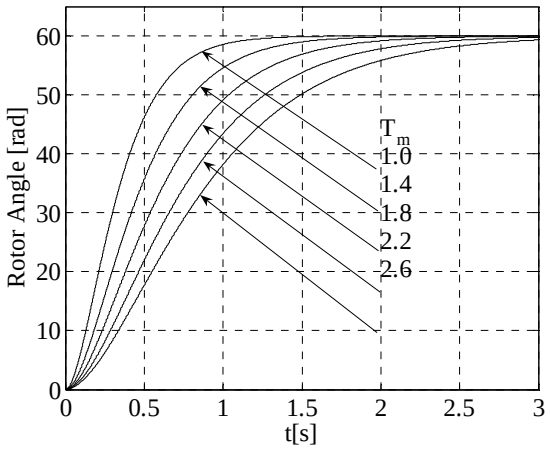

Fig. 9: Position responses with conventional linear state feedback control for different manoeuvre times.

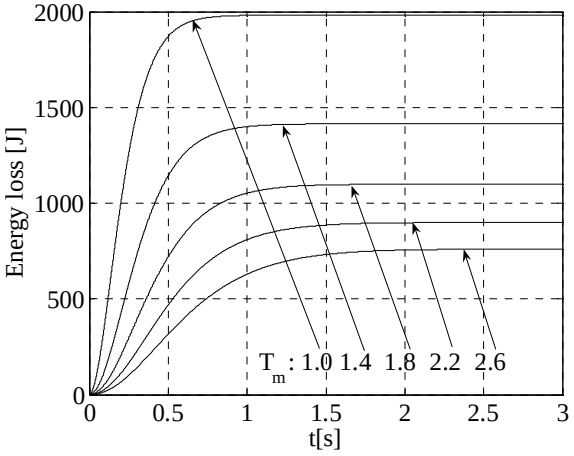

Fig. 10: Energy loss with conventional linear state feedback control for different manoeuvre times.

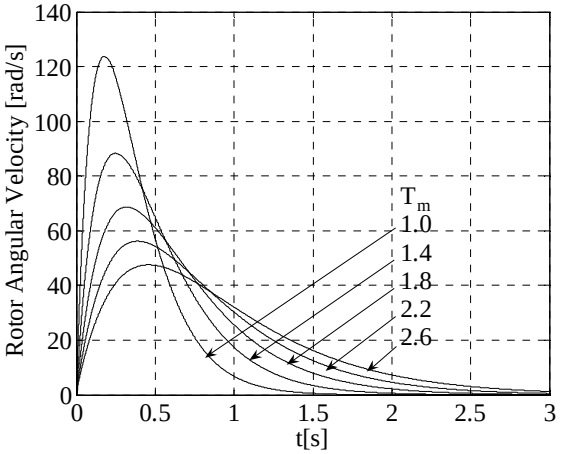

Fig. 11: Energy expenditure for different manoeuvre times with conventional linear state feedback.

The parameters of the non-salient PMSM are:

Rated voltage: $V_0 = 430\,V$; Rated Power: $P_r = 12000\,W$;
Base speed: $\omega_b = 150\,rad/s$; Maximum torque: $\Gamma_{max} = 40\,Nm$; $\Psi_{PM} = 0.38\,Wb$; $L_d = L_q = 5.4e-3H$; $R_s = 0.1\Omega$; $p = 5$; $J_r = 300e-4\ Kg\,m^2$.

The parameters of the mechanical load referred to the PMSM rotor are: $J_L = 4J_r$;
The coefficient of viscous friction is equivalent to 80% of the maximum load power: $F_v = 0.8\,P_r/\omega_b^2$.

The FDC inner loop parameters are as follows: $T_{si} = 5e-3s$; $T_{s\alpha} = 1e-3s$; $T_{so} = 2e-4$.

The outer position control loop parameters are as follows:
Maximum acceleration magnitude: $\alpha_{max} = H.P_r/V_0$;
Sliding mode time constant: $T_c = 0.005s$.
Boundary layer gain: $K = 1000$;

Figs. 6 to 10 show the results for a rest-to-rest manoeuvre with a fixed demanded angle of $\theta_r = 60\,rad$ using the new sliding mode forced dynamic control law. This requires nearly 10 rotor revolutions, which is realistic for motion control applications. Fig. 8 shows the corresponding speed responses. The energy expenditure penalty for reducing the settling time is evident in Fig. 7. As expected, the velocity-time profiles of Fig. 9 are of the form depicted in Fig. 4 and exhibit the increase in the peak angular velocities responsible for the frictional energy loss and the manoeuvre time is reduced. The initial angular acceleration is relatively high so that on the time scale of the figure, the initial linear ramps to the peak velocity values are hardly visible but the final exponential decay of the velocities to zero may be seen.

For comparison, Figs 9, 10, and 11 show the graphs corresponding, respectively, to Figs 6, 7 and 8, obtained using a conventional linear state feedback control law

$$u = g_1\left(\theta_{r\,dem} - \hat{\theta}_r\right) + g_2\hat{\omega}_r \tag{62}$$

with the gains determined by coincident pole placement to yield the same manoeuvre times for critical damping using the Dodds 2% settling time formula [4]:

$$s^2 + g_2 s + g_1 = \left[s + \frac{4(3+2n)}{5T_m}\right]^n\Bigg|_{n=2} = s^2 + \frac{56}{5T_m}s + \frac{784}{25T_m^2} \Rightarrow$$

$$\begin{cases} g_1 = \dfrac{784}{25T_m^2}, & g_2 = \dfrac{56}{5T_m} \end{cases} \tag{61}$$

Similar results would be expected using traditional PI controllers for cascaded speed and position control loops adjusted to yield zero overshoot and the same manoeuvre times.
Comparison of Fig. 7 with Fig. 10 indicates a significant reduction of energy loss using the FDSMC controller for all the demanded manoeuvre times. Table 1 shows the percentage energy savings for each case.

Table 1: Percentage energy savings relative to conventional controller for different manoeuvre times

T_m [s]	1.0	1.4	1.8	2.2	2.6
% Energy Saving	27.9	27.8	27.5	26.8	25.1

The reason for this is the characteristically large initial velocity peak produced by the conventional control law that is about twice the peak velocity produced by the FDSMC controller.

The small overshoots in Fig. 7 are due to some of the kinetic energy stored in the rotor/driven mechanism being returned to the power supply during deceleration.

6 Conclusions and Recommendations

A new closed loop position controller for vector controlled PMSM drives has been proposed that offers considerable advantages over currently employed conventional controllers. First it yields lower frictional energy losses: an energy saving of the order of 27%. If such a controller were to be adopted throughout industry, the energy saving would have a significant positive impact on the environment. Also the system is potentially very practicable in view of its ability to precisely realise a demanded manoeuvre time for a given position demand without the need to model the mechanical load. Applications would include coordinated control of mechanisms and multi-axis machines on production lines. The elimination of the need for time consuming adjustment of PI controllers by trial and error at commissioning time is also a considerable advantage.

In view of the generality of the FDC and SMC methods, it is clear that the new controller is not restricted to PMSM drives and therefore investigation of its application to drives employing other types of motor is recommended.

Experimental trials will be the next step of the research. Also, a further investigation in which the true optimal control that absolutely minimises the

energy expenditure is determined, even if it is only computed on an open loop basis, would be of interest to provide a standard of comparison for the proposed control system.

7 Acknowledgement

The authors wish to thank Control Techniques Dynamics, Walworth Industrial Estate, Andover, UK, for sponsorship of this research

References:

[1] Ma, S., Real-time algorithm for quasi-minimum energy control of robotic manipulators *Industrial Electronics, Control, and Instrumentation*, 1995., Proceedings of the 1995 IEEE IECON 21st International Conference on Volume 2, Issue 6-10 Nov 1995 pp. 1324 – 1329.

[2] Vittek, J. and Dodds, S. J.: '*Forced Dynamics Control of Electric Drives*', EDIS, Žilina University Publishing Centre, 2003, ISBN 80-8070-087-7.

[3] Dodds, S. J., 'Forced Dynamic Control: A Model Based Control Technique Illustrated by a Road Vehicle Control Application', *Proceedings of AC&T 2006*, SCOT, University of East London, UK, ISBN 0-9550008-1-5.

[4] Dodds, S. J., 'Settling Time Formulae for the Design of Control Systems with Linear Closed Loop Dynamics', *Proceedings of AC&T 2008*, SCOT, University of East London, UK, ISBN-10, 0-9550008-5-8.

[5] Utkin, V. I., (1992). *'Sliding Modes in Control Optimization'*, Springer-Verlag, 1992, ISBN 9780387535166.

[6] Ryan, E.P., *'Optimal Relay and Saturating Control System Synthesis'*, Peter Peregrinus, ISBN: 0-90604-856-7 & 978-0-90604-856-6.

[7] Dodds, S. J., 'Observer Based Robust Control', *Proceedings of AC&T 2007*, SCOT, University of East London, UK, ISBN 0-9550008-3-1.

[8] Stadler, P. A., Dodds, S. J. and Wild, H., 'Observer Based Robust Control of a Linear Motor Actuated Vacuum air Bearing', *Proceedings of AC&T 2007*, SCOT, University of East London, UK, ISBN 0-9550008-3-1.

[9] Pontryagin, L. S., Boltyanskii, V. G., Gamkrelidze, R. V., and Mishchenko, E. F., *The Mathematical Theory of Optimal Processes*, 1964, Pergamon.

[10] Isidori, A., *Nonlinear Control Systems*, 3rd Edition, Springer-Verlag, 1995.

[11] Dodds, S. J. and Szabat, K., 'Forced Dynamic Control of Electric Drives with Vibration Modes in the Mechanical Load', *Proceedings of EPE-PEMC '06*, Portoroz, Slovenia.